Dalton Transactions

PAPER

View Article Online
View Journal | View Issue

Cite this: *Dalton Trans.*, 2015, **44**, 7373

Dehydrogenation of ammonia-borane by cationic Pd(II) and Ni(II) complexes in a nitromethane medium: hydrogen release and spent fuel characterization†

Sung-Kwan Kim,[a] Sung-Ahn Hong,[a] Ho-Jin Son,*[a] Won-Sik Han,[b] Artur Michalak,[c] Son-Jong Hwang*[d] and Sang Ook Kang*[a]

Received 10th February 2015,
Accepted 10th March 2015

DOI: 10.1039/c5dt00599j

www.rsc.org/dalton

A highly electrophilic cationic Pd^{II} complex, $[Pd(MeCN)_4][BF_4]_2$ (**1**), brings about the preferential activation of the B–H bond in ammonia-borane ($NH_3{\cdot}BH_3$, AB). At room temperature, the reaction between **1** in CH_3NO_2 and AB in tetraglyme leads to Pd nanoparticles and formation of spent fuels of the general formula $MeNH_xBO_y$ as reaction byproducts, while 2 equiv. of H_2 is efficiently released per AB equiv. at room temperature within 60 seconds. For a mechanistic understanding of dehydrogenation by **1**, the chemical structures of spent fuels were intensely characterized by a series of analyses such as elemental analysis (EA), X-ray photoelectron spectroscopy (XPS), solid state magic-angle-spinning (MAS) NMR spectra (^2H, ^{13}C, ^{15}N, and ^{11}B), and cross polarization (CP) MAS methods. During AB dehydrogenation, the involvement of $MeNO_2$ in the spent fuels showed that the mechanism of dehydrogenation catalyzed by **1** is different from that found in the previously reported results. This AB dehydrogenation derived from $MeNO_2$ is supported by a subsequent digestion experiment of the AB spent fuel: $B(OMe)_3$ and *N*-methylhydroxylamine ($[Me(OH)N]_2CH_2$), which are formed by the methanolysis of the AB spent fuel ($MeNH_xBO_y$), were identified by means of ^{11}B NMR and single crystal structural analysis, respectively. A similar catalytic behavior was also observed in the AB dehydrogenation catalyzed by a nickel catalyst, $[Ni(MeCN)_6][BF_4]_2$ (**2**).

Introduction

Effective storage and release of hydrogen are very important for practical applications in hydrogen fuel-cell vehicles.[1–3] Ammonia borane (NH_3BH_3, AB) has received considerable attention as an outstanding candidate for chemical hydrogen storage due to its low thermolysis temperature,[4] high gravimetric storage density, high stability under normal fuel cell operating conditions, non-toxicity,[5–7] and recently realized regeneration from the spent fuel.[8] The total hydrogen content of AB is 19.6 wt%, or 6.5 and 13.1 wt% for the first and second equivalents of hydrogen released, respectively, potentially securing the ultimate targets of the DOE (7.5 system wt%).[9] A high-performance dehydrogenation catalyst that can facilitate the fast yet efficient release of hydrogen at low temperatures is highly needed for the development of efficient on-board hydrogen storage materials based on AB. In this respect, several types of dehydrogenation catalysts have been developed, where H_2 evolution is mainly catalyzed by a wide range of homogeneous transition metal catalysts, such as rare transition metal catalysts (ruthenium,[10] rhodium,[11] and iridium[12]) as well as more abundant metals such as group 4 organometallics,[13] nickel,[14] iron,[15] and group 6 metal carbonyls.[16] Group 10 transition metal complexes also have been exploited to achieve this target: only a few results are represented by the Ni^0-Enders' NHC (1,3,4-triphenyl-4,5-dihydro-1*H*-1,2,4-triazol-5-ylidene) complex,[14,17] and nanostructured Pd^0 heterogeneous systems[18] that release 2–2.5 equivalents of hydrogen from AB. Recently, we have reported dehydrogenation kinetics by the Pd^{II} complex $[Pd(MeCN)_4][BF_4]_2$ (**1**) with a 2.0 equiv. of H_2 release at room temperature within 60 seconds.[19] However, in comparison with the rapidly growing number of catalysts,

[a]*Department of Advanced Materials Chemistry, Korea University, Sejong 339-700, Korea. E-mail: hjson@korea.ac.kr, sangok@korea.ac.kr*
[b]*Department of Chemistry, Seoul Women's University, Hwarang-ro 621, Seoul, Korea*
[c]*Department of Theoretical Chemistry, Faculty of Chemistry, Jagiellonian University, R. Ingardena 3, 30-060 Kraków, Poland*
[d]*Division of Chemistry and Chemical Engineering, California Institute of Technology, Pasadena, CA 91125, USA. E-mail: sonjong@cheme.caltech.edu*

†Electronic supplementary information (ESI) available: (S1 and S2) X-ray photoelectron spectroscopy (XPS) and IR spectra of the spent fuel. (S3) ^{11}B MAS NMR spectrum of the spent fuel. (S4) Digestion procedures of the spent fuel. (S5 and S6) ^{13}C MAS, CPMAS, 1D ^{11}B MAS, and 2D ^{11}B MQMAS NMR spectra of the spent fuel. See DOI: 10.1039/c5dt00599j

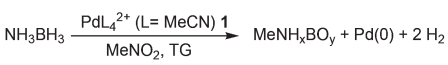

Scheme 1 Formation of AB dehydrocoupling products ($MeNH_xBO_y$) with the $[Pd(MeCN)_4][BF_4]_2$ (**1**) catalyst.

the amount of experimental studies that deal with mechanistic details is still limited.

With this in mind, we present a comprehensive experimental study on the mechanism of AB dehydrogenation with the $[Pd(MeCN)_4][BF_4]_2$ (**1**) catalyst, which exhibited quite high activity (releasing more than 2 equiv. of H_2) in our previous report.[19] In addition to imparting the efficient dehydrogenation ability of **1**, we discovered that the dehydropolymerization forms mostly B–B bonds in a less regular process with the preferential activation of B–H bonds, but did not further investigate the structural elucidation of the spent fuel for mechanism analysis in a recent preliminary communication.[19] We initially thought that the composition of the dehydropolymerized product could be similar to other reported AB spent fuels ($[H_2NB]_n$).[10,14] To our surprise, it is observed *via* solid state NMR analysis that there exists a sizable amount of carbon and oxygen in the spent fuel besides B and N, indicating that C and O atoms are incorporated into the solvent used during AB dehydrogenation or an external environment such as H_2O (in air) after AB dehydrogenation – *albeit*, to a much lesser extent than the solvent (Scheme 1). For this reason, we sought other explanations. In an effort to follow a mechanistic pathway of dehydrogenation, the spent fuels, which are solid residues precipitated after AB dehydrogenation, were characterized in detail by the solid state magic-angle-spinning (MAS) NMR spectroscopy (^2H, ^{13}C, ^{15}N, and ^{11}B) and cross polarization (CP) magic angle spinning NMR. A subsequent digestion step of the spent fuel by methanolysis enabled their exact chemical species to be characterized by typical characterization tools such as single crystal X-ray and NMR analyses. On the basis of such analyses, it is rationalized that $MeNO_2$ is used as the main source of carbon and oxygen in the spent fuel network, and its origin is clearly confirmed with a mechanistic study of deuterium tracing (^2H MAS NMR). In addition, to explore the generality of this mechanistic pathway, AB dehydrogenation by a nickel catalyst, $[Ni(MeCN)_6][BF_4]_2$ (**2**) was performed. As compared to the palladium catalyst, the nickel catalyst (**2**) was less active in AB dehydrogenation releasing only 1.8 equiv. of H_2 at 80 °C over the extended periods (60 minutes). Both palladium (**1**) and nickel (**2**) catalysts are believed to participate in the reaction with the same dehydrogenation sequence to produce similar spent fuels called borates. Herein, the results of the mechanistic studies of these reactions are presented.

Experimental section

Materials and methods

All of the experiments were carried out under a nitrogen atmosphere using the Schlenk techniques or in a Vacuum Atmosphere HE-493 drybox. The solvents were dried over Na (tetraglyme), Na/benzophenone (THF), $CaCl_2$ (nitromethane), and CaH_2 (methanol) distilled under nitrogen and deoxygenated prior to use. The deuterated solvents were dried by trap to trap distillation from CD_3NO_2 ($CaCl_2$), Na (C_6D_6) and CaH_2 (CD_3Cl, CD_3OD) and deoxygenated using three freeze–pump–thaw cycles. A palladium sponge and nitrosonium tetrafluoroborate were purchased from Strem Chemicals. Catalysts **1** and **2** were prepared as described in the literature.[20]

Analytical methods

The solution NMR spectra were recorded at room temperature using a Varian Mercury-300BB spectrometer unless otherwise stated. The ^{11}B NMR spectra were referenced to an external sample of $BF_3{\cdot}Et_2O$ set to 0 ppm. For solid state MAS NMR spectroscopy, the samples were packed under an Ar gas atmosphere into a 4 mm ZrO_2 rotor that was sealed with a tight fitting Kel-F cap inside of a glovebox. The spectra were recorded using a Bruker DSX-500 spectrometer and a boron-free 4 mm Bruker CPMAS probe. Sample spinning was performed using a dry N_2 gas. The spectral frequencies were 500.23, 160.5, 50.7, and 76.8 MHz for ^1H, ^{11}B, ^{15}N, and ^2H nuclei, respectively. One dimensional ^{11}B MAS spectra were recorded after a 0.5 μs pulse ($<\pi/12$) with the application of a strong ^1H decoupling pulse. ^{11}B multiple-quantum (MQ) MAS NMR spectra were recorded by employing the standard *Z*-filtered scheme[21] and presented after the shearing transformation.[22] Spectral decomposition and fittings were performed using the Quasar routine in the DMFIT[23] software. The IR spectra were recorded on a Nicolet Avatar 330 FT-IR spectrometer with a KBr pellet. The elemental analyses were performed using a CE Instruments/Thermo Quest Italia Flash EA 1112 Series. Inductively coupled plasma-atomic emission spectroscopy was performed using a Varian 710-ES Model.

The spent fuel solid samples were analyzed using field-emission transmission electron microscopy (TEM, FEI TECNAI G2 200 kV and Jeol JEM 2100F), electron diffraction (ED), and energy-dispersive X-ray fluorescence spectroscopy (EDX). The X-ray diffraction (XRD) patterns were obtained using the 8C2 and 3C2 beam lines of the Pohang Light Source (PLS) with a monochromatic radiation (λ = 1.54520 Å). X-ray photoelectron spectroscopy (XPS) was carried out using the 8A1 beam line of the Pohang Light Source (PLS) and a laboratory-based spectrometer (VG Scientifics ESCALAB 250) with a photon energy of 1486.6 eV (Al Kα).

The quadrupole mass spectroscopy (QMS) data were obtained using a SRS (Stanford Research Systems) RGA200 quadrupole mass spectrometer that was attached to a glass vacuum line system.

A Quattro Micro triple quadrupole instrument that was equipped with an electrospray ionization source (Waters Corporation, Milford, MA, USA) was used in the negative and positive ionization mode. The sample solution was directly infused at a flow rate of 100 μL min^{-1} using a syringe pump. The scanning mass range of the mass spectrometer was 5–2000 Da with a step size of 0.5 Da. The capillary voltage and

the cone voltage were set at 3200 V and 15–25 V respectively, with nitrogen as the drying gas. The desolvation gas flow was 350 L h^{-1} and the cone gas flow was 70 L h^{-1}. The desolvation temperature was 350 °C and the source temperature was 100 °C.

General procedure of AB dehydrogenation

Apparatus and procedure for the Pd(II) catalyzed dehydrogenation

The reactor consisted of modified 50 mL double jacket glassware. A three way connector was modified to purge the system with argon gas and allowed the hydrogen gas that was produced during the reaction to pass through the mass flow meter. This system enabled the catalyst to be injected into the reactor without exposing the reactants to air. The reaction temperature was monitored and controlled using a thermocouple and an external heater/cooler, respectively. The experimental procedure involved filling the reactor with 2 mL of the tetraglyme solution containing 1.46 mmol of AB. The reactor was subsequently flushed with argon for at least 30 min in order to minimize the moisture level inside the vessel. After the thermal equilibration between the reactor and the cold trap, 3 mol% of catalyst **1** was dissolved in 0.5 mL nitromethane ($MeNO_2$) and injected into the AB solution. The reaction time was calculated from the time when the catalyst was introduced into the mixture. The progress of the reaction was monitored by examining the amount of hydrogen that was generated using a volumetric technique, which was used for the real time tracking of the reaction. $MeNO_2$ (bp 101 °C) or other volatiles including NH_3 in the product stream were anticipated because of the large exotherm under the experimental conditions even though the temperature was controlled at 25 °C. In the apparatus setup, a −90 °C cold bath (liquid N_2 with CH_2Cl_2) trapped the volatiles to ensure that the volume that was measured using the mass flow meter was only due to hydrogen. After the dehydrogenation, the solid was collected by filtration, rinsed with Et_2O and dried *in vacuo*. The possibility of a heterogeneous pathway was examined either by the supplementary addition of AB after dehydrogenation or mercury poisoning because of the fast hydrogen release kinetics for **1**. Both experiments indicate the presence of a homogeneous catalysis: these successive dehydrogenations with a second charge of AB are slowed due to consumption and partial decomposition (to Pd(0)) of **1** during this catalytic reaction.[11c]

Results and discussion

Catalytic dehydrogenation of AB in tetraglyme with $[Pd(MeCN)_4][BF_4]_2$ (1) in $MeNO_2$ and characterization of spent fuels

It has been a general notion that a coordinating solvent must be avoided due to the electrophilic nature of the cationic catalyst center. For this reason, MeCN was not considered as an appropriate solvent in the first place. In our earlier report, $MeNO_2$ used as a solvent for dissolving **1** because **1** with weakly coordinating acetonitrile ligands is stable only in non-coordinating high polar solvents and insoluble in most organic solvents except MeCN.[19] Before AB dehydrogenation, we checked that **1** is stable and unreactive in $MeNO_2$: neither **1** nor AB was reactive with $MeNO_2$ at room temperature. Only when these three reagents were brought together, a notable dehydrogenation occurred. When 3 mol% of **1** in $MeNO_2$ solution was added to a stirred tetraglyme solution containing AB at 25 °C, a vigorous hydrogen evolution with a typical strong exotherm was observed, resulting in 2.0 equiv. of H_2 release within 60 s. During AB dehydrogenation, the insoluble by-products were co-precipitated with Pd particles from the $MeNO_2$ and tetraglyme solution. The insoluble spent fuel was subsequently characterized as the preliminary composition of $B_{1.00}C_{1.09}N_{0.95}H_{4.50}Pd_{0.024}$ by inductively coupled plasma (ICP)/elemental analysis (EA), and as $B_{1.00}C_{1.40}N_{0.65}O_{1.89}Pd_{0.05}$ by X-ray photoelectron spectroscopy (XPS) (see Table 1 and Fig. S1†). From these analyses, we found that a significant amount of carbon and oxygen was incorporated into the BNH_x matrix: an expected chemical composition in spent fuels that is comparable with those of original boron and nitrogen. Further structural characterization by the infrared (IR) spectrum revealed the preferential activation of B–H bonds. As shown in Fig. S2,† the characteristic B–H peaks at around 2300 cm^{-1} in AB have disappeared completely, indicating the preferential B–H activation mechanism.

Fig. 1 and Table 2 present high resolution solid state ^{11}B MAS NMR, 2D multiple quantum (MQ) MAS NMR spectra of the spent fuels, and ^{11}B peaks from the decomposition of 1D MAS NMR spectra, respectively. The 2D-^{11}B MQMAS NMR spectrum was obtained to sort out the inequivalent boron sites that are indistinguishable in the 1D MAS spectrum. Two groups of peaks were initially sorted out by this method. The broad peaks between 10 and 20 ppm originate from boron atoms in the trigonal geometry of BO_3 units while several sharp peaks in the 6 to −6 ppm range were due to boron atoms in the tetrahedral coordination. These sp^3 are believed to be responsible for tetragonal BO_4 units. Based on the 2D MQMAS spectrum, the 1D spectrum was decomposed to 7 different sites as shown in Fig. 1. The peaks are compiled in Table 2. Note that an additional resonance is seen at −10 ppm (see the 2D spectrum) but was ignored due to its negligible contribution. The 1D ^{11}B MAS spectrum without ^{1}H decoupling allowed us to conclude that nearly all boron peaks except the peak at −6 ppm (and −10 ppm) are without direct B–H bonds. However, these peaks showed high efficiency (intensity) in ^{1}H–^{11}B cross polarization MAS NMR (see Fig. 1), indicating that the boron atoms are in close proximity to either NH or –CH organic species. The ratio of $[B]_{trigonal}$ *vs.* $[B]_{tetrahedral}$ ($B^3 : B^4$) was calculated to be 2 : 3 from the spectral decomposition, which allows speculation about a possible structure. Lastly, the fairly sharp peak at −1.6 ppm is believed to be BF_4^- although its binding cation is not known. As shown in Table 2,

Table 1 Elemental analysis and formula of the spent fuel

	Spent fuel components						
Method	B	C	N	O	H	Pd	Formula of spent fuel
EA[a]	—	1.09	0.95	—	4.50	—	$B_{1.00}C_{1.09}N_{0.95}H_{4.50}Pd_{0.024}$
ICP[b]	1.00	—	—	—	—	0.024	
XPS[c]	1.00	1.40	0.65	1.89	—	0.05	$B_{1.00}C_{1.40}N_{0.65}O_{1.89}Pd_{0.05}$

[a] Elemental analysis. [b] Inductively coupled plasma-atomic emission spectroscopy. [c] X-ray photoelectron spectroscopy.

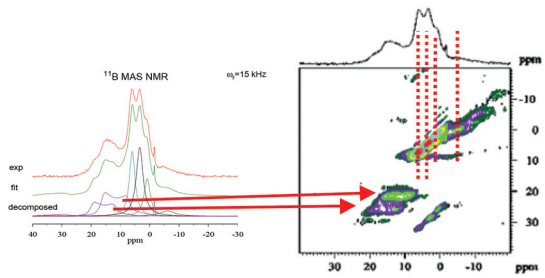

Fig. 1 1D ^{11}B MAS (left) and 2D ^{11}B MQMAS (right) NMR spectra of the spent fuel.

Table 2 ^{11}B peaks from deconvolution of 1D and 2D MAS NMR spectra

Chemical shift (δ_{iso})	C_q[a] (MHz)	η	Relative intensity ratio	
21.9	2.53	0.1	0.13	sp^2: 0.37
18.5	2.70	0.1	0.24	
6.2	0.5	1	0.20	sp^3: 0.57
3.6	0.5	1	0.25	
1.1	0.5	1	0.12	
−6.0	0.5	1	0.04	BH_x
−1.6	—	—	<0.01	BF_4^-

[a] C_q: quadrupole coupling constant (= eq^2Q/h); η: asymmetry parameter (= $(V_{xx} - V_{yy})/V_{zz}$), where their usual definition can be readily found for the quadrupole interaction in magnetic resonance.[25]

^{11}B NMR of the AB spent fuel showed a mixture of two trigonally (sp^2) and tetrahedrally (sp^3) coordinated boron atoms. The trigonal boron atoms are clearly distinctive from those of BN_3, BN_2H type of sp^2 boron sites of polyborazylene, or BN[24] in comparison with the simulated spectra of BN, BN_2H, and $B(OH)_3$, which are plotted together with the experimental data (see Fig. 1 and S2†).

In addition to the routine probing nuclei such as ^{1}H and ^{11}B, the chemical transformation of the B–N bond of AB was further explored by ^{15}N NMR spectroscopy. The ^{15}N labelled AB[27] was used for this purpose and the same catalytic reaction was performed using the Pd catalyst and the spent fuel under the same conditions that have been used in the case of an unlabelled AB (see above). The corresponding ^{15}N MAS and CPMAS NMR spectra of ^{15}N-sfAB samples are shown in Fig. 2.

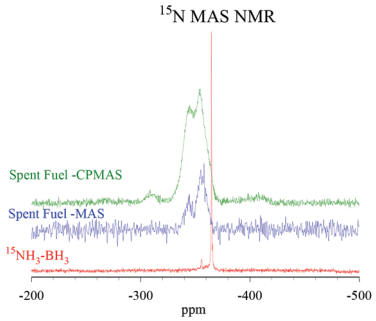

Fig. 2 ^{15}N MAS and CPMAS NMR spectra of sfAB that was generated using ^{15}N labelled AB ($^{15}NH_3$–BH_3). Note that the vertical scale of $^{15}NH_3$–BH_3 was adjusted by 1/100 for the purpose of comparison. The ^{15}N shift was externally referenced to neat CH_3NO_2.

The ^{15}N signal of the remaining nitrogen compound in the spent fuel showed two major peaks at −340.5 and −353 ppm with an intensity ratio of 1 : 3. While the signal by MAS alone is weak and a time-consuming experiment to obtain the spectrum with a good signal to noise ratio due to a long relaxation time and low nitrogen quantity, the ^{1}H–^{15}N cross polarization (CP) method appears to improve the signal quality markedly and a more detailed spectral analysis is possible. The CPMAS method made the small and broad resonances at −310 and −410 ppm, which were invisible in the MAS spectrum. Typically peaks in the −250 to −330 ppm range represent nitrogen atoms that are trigonally coordinated while those in the −330 to −400 ppm range are attributed to N atoms in the tetrahedral coordination.[26] According to Gervais *et al.* and the references cited therein, NB_3 sites appear between −250 and −300 ppm. As shown in Fig. 2, besides the small peak nearly at −310 ppm, most of the N containing species of sfAB can be associated with tetrahedrally coordinated N sites that are typically found in PAB ($–NH_2BH_2–$).[27] The corresponding ^{11}B signal, tetrahedrally coordinated B sites and especially those peaks at ~−10 ppm, explains the remaining B–N moieties in the spent fuel. The −310 ppm peak might show the presence of B_2NH trigonal sites in a hexagonal ring structure as shown there. Note, however, that among the ^{15}N signals, its contribution is negligibly small. It is not yet clear about a possible local structure of N sites that could represent the −410 ppm peak. Again, its contribution is negligible.

Catalytic dehydrogenation of AB in tetraglyme with 1 in $MeNO_2$-d_3 and characterization of spent fuels

In an effort to elucidate the incorporation of $MeNO_2$ into a spent fuel framework, an experiment using deuterium tracing was performed *via* ^2H MAS NMR analysis with $MeNO_2$-d_3 (CD_3NO_2) employed as a solvent to dissolve **1**. As soon as 3 mol% of **1** dissolved in $MeNO_2$-d_3 was added to a stirred tetraglyme solution containing AB at 25 °C, fast AB dehydrogenation was observed as expected, completing a 2.0 equiv. of H_2 release in 60 s. The dehydrogenated products were co-precipitated with Pd particles from the $MeNO_2$-d_3 and tetraglyme solution.

Structural characterization of the precipitant is obtained by ^2H MAS NMR analysis. The majority of signals is due to the $-CD_3$ moiety showing a C_3 free rotational motion, indicated by the quadrupole coupling constant (C_q = 54 kHz) determined from a spectral fit of the experimental spectrum (see Fig. 3a), and this could be bound to the boron compounds *via* a reduced NO_2 group. It is observed that there exist three different deuterium species: besides the CD_3- at 0.4 ppm (C_q = 54 kHz, dominating >70%), there are a CD- group (immobile, 5.7 ppm, C_q = 171.4 kHz, 17%) and a solvent like mobile CD_3NO_2 phase (4.8 ppm, C_q = 10 kHz, 12%, see Fig. 3b).

In high resolution solid state ^{11}B MAS NMR analysis, we found that the peaks of the $MeNO_2$-d_3 mediated AB spent fuel are similar to those of the non-deuterated solvent system, which is described in our earlier discussion part (Fig. 1 and Table 2), showing identical kinetics of the deuterated and non-deuterated $MeNO_2$ solvent system. ^{11}B peaks from the decomposition of 1D and 2D MAS NMR spectra is summarized in Table 3. As shown in Fig. 4, 1D ^{11}B MAS NMR spectra clearly show the simplest and clean line shape of the BO_3 units at around 18 ppm. The Q_{cc} and eta parameters are classified into two different kinds of families. Several sharp peaks in the 4 to −2 ppm range represent borons in the tetrahedral coordination, which are believed to be responsible for tetragonal BO_4 units. The broad peak at −8 to −16 ppm is assigned as a possible location for BH_2 units, implying the incomplete dehydrogenation.

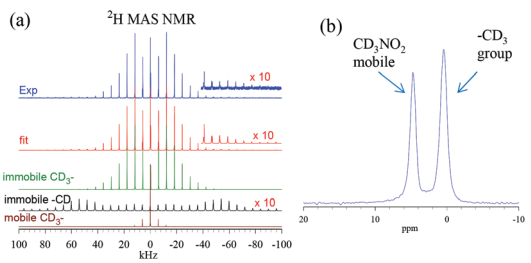

Fig. 3 ^2H MAS NMR of the spent fuel from dehydrogenation of AB in tetraglyme by **1** in $MeNO_2$-d_3, (a) experimental ^2H MAS spectrum at a spinning rate of 6 kHz, a fitted spectrum, and the corresponding 3 components, (b) the center band. The presence of an immobile C–D group is manifested by a powder pattern (see ×10 scaled portion) of a typical C–D quadrupole interaction (C_q = 171.4 kHz). The shift in ppm was referenced to D_2O at 4.7 ppm.

Table 3 ^{11}B peaks from decomposition of 1D and 2D MAS NMR spectra

Shift	Q_{cc} (MHz)	eta	Rel. int. ratio	
18.01	2.52	0.1	0.45	sp^2
3.62	0.5	1	0.08	sp^3
2.05	0.5	1	0.14	
0.74	0.5	1	0.22	
−1.62	0.2	1	0.04	
−7.5	0.5	1	0.01	
−9.44	0.5	1	0.01	
−11.57	0.5	1	0.01	
−15.4	0.5	1	0.04	

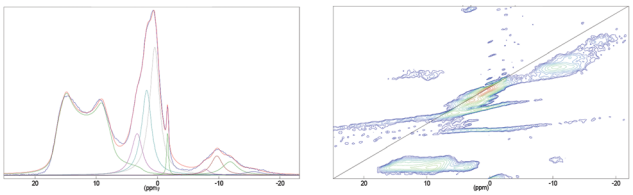

Fig. 4 1D ^{11}B MAS (left) and 2D ^{11}B MQMAS (right) NMR spectra of spent fuels from dehydrogenation of AB in tetraglyme by **1** in $MeNO_2$-d_3.

The reactivity of AB with $MeNO_2$ and characterization of spent fuels

For the insight of the cross reactivity between AB and $MeNO_2$, AB dehydrogenation by $MeNO_2$ is performed without Pd catalyst **1** and tetraglyme solvent. We observed a trace amount of the released gas over the extended periods (10 h at 25 °C). We tested the $MeNO_2$-mediated performance, plotting the amount of H_2 released with different reaction temperatures (25, 60, 80, and 100 °C). Up to 60 °C, no discernible H_2 production was noted, but that observed in 80 °C to 100 °C temperature is the detectable dehydrogenation with white precipitations, which are insoluble in most aprotic solvents.

The precipitates (S1) produced from AB dehydrogenation without **1** and tetraglyme are also characterized by ^1H and ^{11}B MAS NMR analysis. For the exact results, it is compared with NMR spectra of both the AB spent fuels ($[CNH_x]BO_y$), which are generated with **1** and tetraglyme in the CH_3NO_2 solvent, and the precipitates (S2) generated with **1** in the CD_3NO_2 solvent (see Fig. 5). Overall, the outcome of both ^1H and ^{11}B MAS NMR spectra for S1 is noticeably different from those of BNH_x. However, the difference is mainly due to the degree of reaction progressed in S1, which was supposedly lower due to the lack of catalyst **1**. The S2 shows simply only one BO_3 peak at 18.4 ppm. The S1 shows the same BO_3 peak with a very small addition of the secondary BO_3 peak at 21.6 ppm (see Table 4). Interestingly, the S1 contains numerous BO_4 peaks covering a wide range from −4 ppm to 6 ppm, seemingly the BO_4 peaks seen for both $[CNH_x]BO_y$ and S2 (see Fig. 5). The BH_2 units at −10 ppm[28] are seen for both S1 and S2 in relatively high concentration, showing the incomplete dehydro-

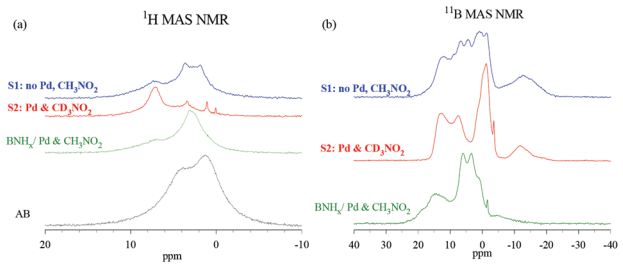

Fig. 5 (a) ^{1}H and (b) ^{11}B MAS NMR spectral comparison for white precipitations of the AB spent fuel with $MeNO_2$ solvents.

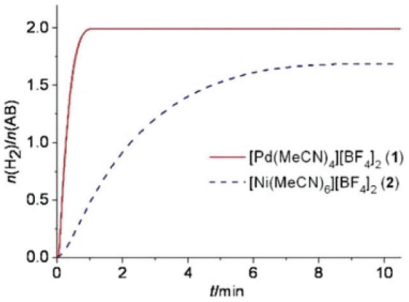

Fig. 6 AB dehydrogenation kinetic profiles for [Pd(MeCN)$_4$][BF$_4$]$_2$ (**1**) at 25 °C in $MeNO_2$ and [Ni(MeCN)$_6$][BF$_4$]$_2$ (**2**) in $MeNO_2$ at 80 °C.

Table 4 ^{11}B peaks from decomposition of 1D and 2D MAS NMR spectra

Shift (ppm)	Q_{cc} (MHz)	eta	Rel. int. ratio
21.9	2.53	0.15	0.03
17.91	2.52	0.15	0.30
11.31	0.5	1	0.01
9.14	0.5	1	0.02
6.69	0.5	1	0.11
3.26	0.5	1	0.25
0.78	05	1	0.10
−7.02	0.5	1	0.03
−10.37	0.5	1	0.08
−13.84	0.5	1	0.06

Table 5 ^{11}B peaks from decomposition of 1D and 2D MAS NMR spectra

Chemical shift (δ_{iso})	C_q	Relative intensity ratio	
21.8	2.6	0.11	sp^2: 0.41
18.4	2.53	0.30	
9.39	0.2	0.04	sp^3: 0.59
6.55	0.2	0.04	
3.57	0.2	0.23	
0.8	0.5	0.16	
−10.08	0.2	0.07	
−14.94	0.2	0.06	

genation. These results strongly support the involvement of CH_3NO_2 in the AB spent fuels.

Catalytic dehydrogenation of AB in tetraglyme with [Ni(MeCN)$_6$][BF$_4$]$_2$ (2) in $MeNO_2$ and characterization of spent fuels

AB dehydrogenation was performed using the [Ni(MeCN)$_6$][BF$_4$]$_2$ (**2**) under the same stated conditions. However, Ni catalyst **2** was inactive under mild conditions, producing only 0.2 and 1.0 equiv. of H_2 (in 2 h) at 25 and 60 °C, respectively. At a slightly increased temperature, 80 °C, 1.8 equiv. of H_2 is released during 60 min (see Fig. 6). Similar to the typical method mentioned above, 3 mol% of **2**, which is dissolved in 0.5 mL of $MeNO_2$, was added to 2 mL of a stirred tetraglyme solution containing 0.045 g (1.46 mmol) of AB at different temperatures. The dehydrogenation product is co-precipitated with Ni particles completely from tetraglyme and $MeNO_2$, which were later found to be insoluble in most aprotic solvents. Except for the dehydrogenation performance, the signs of a reaction including the production of precipitation are similar to the case of Pd catalyst **1**.

^{11}B MAS NMR spectra of the spent fuel produced by **2** in $MeNO_2$ reveal very similar features to that by **1** as described in Table 5 and Fig. 7. Two groups of peaks were initially sorted out by this method. The broad peaks between 10 and 20 ppm are apparently assigned as boron atoms in the trigonal geometry of BO_3 units, while several sharp peaks ranging from 6 to −6 ppm can be assigned as boron atoms in a tetrahedral

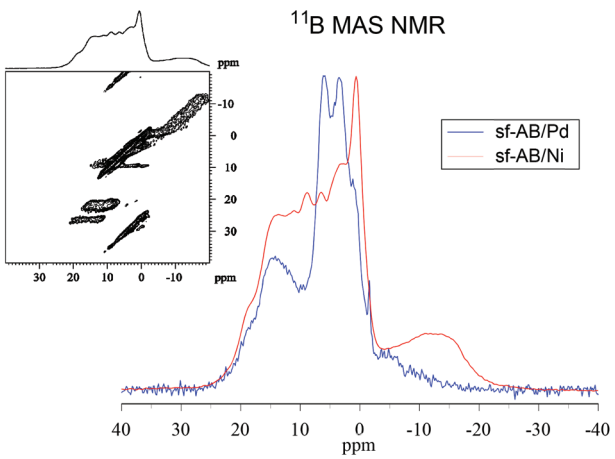

Fig. 7 Comparison of 1D ^{11}B MAS and 2D ^{11}B MQMAS (inset) NMR spectra of spent fuels produced by **1** and **2** catalysts in $MeNO_2$/tetraglyme solution.

coordination. These sp^3 are believed to be responsible for tetragonal BO_4 units. Similar to those found in the cases of S1 and S2, the broad peaks at −10 to −15 ppm are assigned as a possible location for BH_2, which means that the incomplete dehydrogenation originated from the relatively low catalytic ability of Ni catalyst **2**. Based on the 2D spectrum, the 1D spectrum was decomposed to 8 different sites as shown in Table 5.

The ratio of $[B]_{trigonal} : [B]_{tetrahedral}$ ($sp^2 : sp^3$) was calculated to be 2 : 3 from the spectral decomposition. Consequently, this spectral similarity in the solid NMR spectra (of spent fuels by **1** and **2**) elucidates a mechanism for the $MeNO_2$-mediated AB dehydrogenation.

Structural characterization by digestion of the spent fuels: Pd-NPs catalyzed methanolysis of $MeNH_xBO_y$

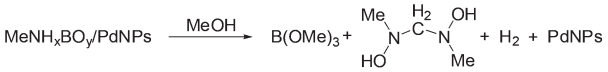

In an effort to analyze the exact chemical species of the spent fuel remaining after AB dehydrogenation, the spent fuel was digested by adding methanol. Digestion of the spent fuel is proceeded with the addition of methanol. Generally Pd nanoparticles have been well known as an effective catalyst for the dehydrogenative methanolysis of AB,[29] and thus the spent fuel ($MeNH_xBO_y$/PdNPs) is used for the impromptu digestion without doing any treatment except the subsequent addition of methanol. All by-products (including releasing gas) generated after the digestion step were fully characterized by NMR, quadrupole mass spectroscopy (QMS), and single crystal X-ray analysis. The ^{11}B NMR chemical shift of 18.1 ppm indicates the formation of $B(OMe)_3$ from the digestion (see Fig. S4 in ESI†). The spent fuel containing the Pd nanoparticles, $MeNH_x$-BO_y/PdNPs (1.07 g, 40 mmol) was placed in a two-neck round-bottom flask that was fitted with a septum inlet and a reflux condenser with a connecting tube. The connecting tube is attached to the mass flow meter *via* a gas bubbler containing 100 mL of water in order to trap the ammonia gas. Gas evolution was detected when methanol (12 mL, 296 mmol) was added to the spent fuel under an argon atmosphere. The released gas was transferred to a QMS that was directly connected to the vacuum line in order to identify the gaseous by-product. Fig. 8 clearly shows that the gas that was released after the addition of methanol solvent is mostly hydrogen. When the hydrogen evolution ceased (64 mL, 2.05 mmol), the aqueous solution of ammonia from the trap was titrated against standard 0.1 N aq. HCl. Only a trace amount of NH_3 was estimated to be 0.0017 g (0.1 mmol). At the end of the reaction, the black solids (0.06 g, 0.563 mmol) were collected

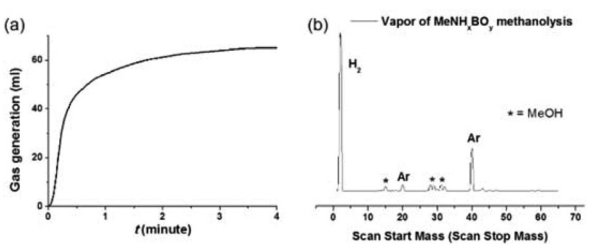

Fig. 8 (a) A H_2 release kinetic profile for the digestion of the spent fuel with the PdNPs and (b) mass spectrum of the volatiles produced by the $MeNH_xBO_y$ methanolysis with the PdNPs. The most intensive mass number detected was m/z = 2 (H_2).

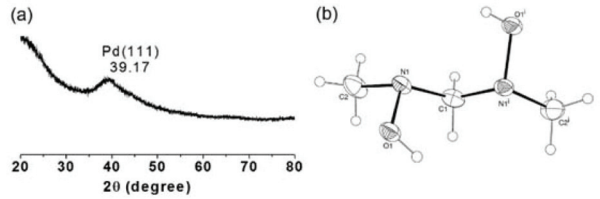

Fig. 9 (a) XRD patterns of the recovered Pd particles from the methanolysis and (b) ORTEP drawing of the molecular structure of $[Me(OH)N]_2CH_2$.

by filtration. The presence of PdNPs was confirmed by the XRD analysis in Fig. 9a. Methanol and $B(OMe)_3$ were recovered from distillation of the filtrate at 69 °C. The ^{11}B NMR spectrum of filtrate clearly shows the exclusive formation of $B(OMe)_3$. Subsequent isolation of $B(OMe)_3$ (1.3 g, 12.51 mmol) from the residue was performed using the trap to trap fractionation under high vacuum (10^{-8} torr) at −30 °C. To analyze the exact composition of the final by-products remaining after the isolation of $B(OMe)_3$, the non-volatile and viscous residue was recrystallized from the methanol solution. From the X-ray structural study of the obtained crystal sample, we realized that the exact chemical structure of the residue is *N*,*N*′-dihydroxy-*N*,*N*′-dimethylmethanediamine ($[Me(OH)N]_2CH_2$) (0.663 g, 6.255 mmol) and they exist as a single product (see Fig. 9b). Consequently, by this digestion experiment of the dehydrogenated products and their further characterization, it is reconfirmed that the AB dehydrogenation by **1** is performed by using a $MeNO_2$ solvent-mediated mechanism and the involvement of the polar solvent in this catalytic reaction is a key step for AB dehydrogenation.

Conclusion

In summary, we have demonstrated that the mechanistic study of AB dehydrogenation by a highly electrophilic cationic Pd^{II} complex (**1**) with structural elucidation of spent fuels. To understand the exact mechanistic pathway, the chemical structure of the spent fuels was fully characterized by solid state magic-angle-spinning (MAS) NMR spectra (^2H, ^{13}C, ^{15}N, and ^{11}B) and cross polarization magic angle spinning (CPMAS). From a series of NMR analyses with a deuterium tracing study (CD_3NO_2), we reasoned that the carbon and oxygen species of $MeNO_2$, which are used as the solvent to dissolve **1**, are significantly involved in formation of the spent fuel, $MeNH_xBO_y$. Two $B(OMe)_3$ and $[Me(OH)N]_2CH_2$ species, which are produced by methanolysis (digestion step) of $MeNH_xBO_y$, are clearly characterized by X-ray crystallography and NMR analysis, providing direct evidence of carbon and oxygen incorporation into spent fuels. In addition, such a mechanism is further generalized by a nickel catalyst, $[Ni(MeCN)_6][BF_4]_2$ (**2**). This work offers the significance and criteria of a non-coordinating polar solvent in the design and development of catalytic AB dehydrogenation

systems. Efforts toward mechanistic investigations as well as performance optimization of an AB catalytic system utilizing different types of polar solvents are currently underway.

Acknowledgements

This work was supported by the New & Renewable Energy Core Technology Program of the Korea Institute of Energy Technology Evaluation and Planning (KETEP) granted financial resource from the Ministry of Trade, Industry & Energy, Republic of Korea (No. 20113030040020) and Basic Science Research Program through the National Research Foundation of Korea (NRF) funded by the Ministry of Education (NRF-2014R1A6A1030732).

Notes and references

1 U.S. DOE, "Hydrogen, Fuel Cells & Infrastructure Technologies Program" (http://www.eere.energy.gov/hydrogenandfuelcells/storage).
2 The American Physical Society, "The Hydrogen Initiative" (http://www.aps.org/public_affairs/index.cfm).
3 L. Schlapbach and A. Züttel, *Nature*, 2001, **414**, 353.
4 F. Baitalow, J. Baumann, G. Wolf, K. Jaenicke-Rößler and G. Leitner, *Thermochim. Acta*, 2002, **391**, 159.
5 H. W. Langmi and G. S. McGrady, *Coord. Chem. Rev.*, 2007, **251**, 925.
6 C. W. Hamilton, R. T. Baker, A. Staubitz and I. Manners, *Chem. Soc. Rev.*, 2009, **38**, 279.
7 A. Staubitz, A. P. M. Robertson and I. Manners, *Chem. Rev.*, 2010, **110**, 4079.
8 (*a*) B. L. Davis, D. A. Dixon, E. B. Garner, J. C. Gordon, M. H. Matus, B. Scott and F. H. Stephens, *Angew. Chem., Int. Ed.*, 2009, **48**, 6812; (*b*) A. D. Sutton, B. L. Davis, K. X. Bhattacharyya, B. D. Ellis, J. C. Gordon and P. P. Power, *Chem. Commun.*, 2010, **46**, 148; (*c*) A. D. Sutton, A. K. Burrell, D. A. Dixon, E. B. Garner III, J. C. Gordon, T. Nakagawa, K. C. Ott, J. P. Robinson and M. Vasiliu, *Science*, 2011, **331**, 1426.
9 (*a*) J. Graetz, *Chem. Soc. Rev.*, 2009, **38**, 73; (*b*) Sigma-Aldrich "Mater. Matters" special issue 2007, volume 2, number 2, http://www.scribd.com/doc/12703635/Hydrogen-Storage-Materials-Material-Matters-v2n2-.
10 (*a*) N. Blacquiere, S. Diallo-Garcia, S. I. Gorelsky, D. A. Black and K. Fagnou, *J. Am. Chem. Soc.*, 2008, **130**, 14034; (*b*) M. Käß, A. Friedrich, M. Drees and S. Schneider, *Angew. Chem., Int. Ed.*, 2009, **48**, 905; (*c*) G. Alcaraz and S. Sabo-Etienne, *Angew. Chem., Int. Ed.*, 2010, **49**, 7170; (*d*) A. N. Marziale, A. Friedrich, I. Klopsch, M. Drees, V. R. Celinski, J. Schmedt auf der Günne and S. Schneider, *J. Am. Chem. Soc.*, 2013, **135**, 13342.
11 (*a*) Y. Chen, J. L. Fulton, J. C. Linehan and T. Autrey, *J. Am. Chem. Soc.*, 2005, **127**, 3254; (*b*) C. A. Jaska, K. Temple, A. J. Lough and I. Manners, *J. Am. Chem. Soc.*, 2003, **125**, 9424; (*c*) C. A. Jaska and I. Manners, *J. Am. Chem. Soc.*, 2004, **126**, 9776.
12 (*a*) M. C. Denney, V. Pons, T. J. Hebden, M. Heinekey and K. I. Goldberg, *J. Am. Chem. Soc.*, 2006, **128**, 12048; (*b*) A. Paul and C. B. Musgrave, *Angew. Chem., Int. Ed.*, 2007, **46**, 8153.
13 (*a*) T. J. Clark, C. A. Russell and I. Manners, *J. Am. Chem. Soc.*, 2006, **128**, 9582; (*b*) D. Pun, E. Lobkovsky and P. J. Chirik, *Chem. Commun.*, 2007, 3297; (*c*) M. E. Sloan, A. Staubitz, T. J. Clark, C. A. Russell, G. C. Lloyd-Jones and I. Manners, *J. Am. Chem. Soc.*, 2010, **132**, 3831; (*d*) T. Miyazaki, Y. Tanabe, M. Yuki, Y. Miyake and Y. Nishibayashi, *Organometallics*, 2011, **30**, 2394; (*e*) T. Beweries, J. Thomas, M. Klahn, D. Heller, A. Schulz and U. Rosenthal, *ChemCatChem*, 2011, **3**, 1865.
14 R. J. Keaton, J. M. Blacquiere and R. T. Baker, *J. Am. Chem. Soc.*, 2007, **129**, 1844.
15 (*a*) J. R. Vance, A. P. M. Robertson, K. Lee and I. Manners, *Chem. – Eur. J.*, 2011, **17**, 4099; (*b*) R. T. Baker, J. C. Gordon, C. W. Hamilton, N. J. Henson, P.-H. Lin, S. Maguire, M. Murugesu, B. L. Scott and N. C. Smythe, *J. Am. Chem. Soc.*, 2012, **134**, 5598; (*c*) J. R. Vance, A. Schafer, A. P. M. Robertson, K. Lee, J. Turner, G. R. Whittell and I. Manners, *J. Am. Chem. Soc.*, 2014, **136**, 3048; (*d*) J. F. Sonnenberg and R. H. Morris, *ACS Catal.*, 2013, **3**, 1092–1102; (*e*) P. Bhattacharya, J. A. Krause and H. Guan, *J. Am. Chem. Soc.*, 2014, **136**, 11153.
16 Y. Kawano, M. Uruichi, M. Shimoi, S. Taki, T. Kawaguchi, T. Kakizawa and H. Ogino, *J. Am. Chem. Soc.*, 2009, **131**, 14946.
17 X. Yang and M. B. Hall, *J. Am. Chem. Soc.*, 2008, **130**, 1798.
18 (*a*) Ö. Metin, S. Duman, M. Dinç and S. Özkar, *J. Phys. Chem. C*, 2011, **115**, 10736; (*b*) R. P. Shrestha, H. V. K. Diyabalanage, T. A. Semelsberger, K. C. Ott and A. K. Burrell, *Int. J. Hydrogen Energy*, 2009, **34**, 2616.
19 S. K. Kim, W.-S. Han, T.-J. Kim, T.-Y. Kim, S. W. Nam, M. Mitoraj, Ł. Piekoś, A. Michalak, S.-J. Hwang and S. O. Kang, *J. Am. Chem. Soc.*, 2010, **132**, 9954.
20 (*a*) R. F. Schramm and B. B. Wayland, *J. Chem. Soc., Chem. Commun.*, 1968, 898; (*b*) T. Lai and A. Sen, *Organometallics*, 1984, **3**, 866.
21 J.-P. Amoureux, C. Fernandez and S. Steuernagel, *J. Magn. Reson., Ser. A*, 1996, **123**, 116.
22 J. P. Amoureux and M. Pruski, in *Encyclopedia of NMR*, ed. D. M. Grant and R. K. Harris, Wiley, 2002, vol. 9, p. 226.
23 D. Massiot, F. Fayon, M. Capron, I. King, S. Le Calvé, B. Alonso, J.-O. Durand, B. Bujoli, Z. Gan and G. Hoatson, *Magn. Reson. Chem.*, 2002, **40**, 70.
24 (*a*) S. Mecking, *Coord. Chem. Rev.*, 2000, **203**, 325; (*b*) C. Gervais, J. Maquet, F. Babonneau, C. Duriez, E. Framery, M. Vaultier, P. Florian and D. Massiot, *Chem. Mater.*, 2001, **13**, 1700; (*c*) J. Li, S. Bernard, V. Salles, C. Gervais and P. Miele, *Chem. Mater.*, 2010, **22**, 2010;

(*d*) C. Gervais, E. Framery, C. Duriez, J. Maquet, M. Vaultier and F. Babonneau, *J. Eur. Ceram. Soc.*, 2005, **25**, 129.

25 D. Freude and J. Haase, Quadrupole effects in solid-state nuclear magnetic resonance, in *NMR Basic Principles and Progress*, ed. P. Diehl, E. Fluck, H. Günther, R. Kasfeld and J. Seelig, Springer-Verlag, Berlin, 1993, vol. 29, p. 1.

26 C. Gervais and F. Babonneau, *J. Organomet. Chem.*, 2002, **657**, 75.

27 W. J. Shaw, J. C. Linehan, N. K. Szymczak, D. J. Heldebrant, C. Yonker, D. M. Camaioni, R. T. Baker and T. Autrey, *Angew. Chem., Int. Ed.*, 2008, **47**, 7493.

28 (*a*) A. C. Stowe, W. J. Shaw, J. C. Linehan, B. Schmid and T. Autrey, *Phys. Chem. Chem. Phys.*, 2007, **9**, 1831; (*b*) J. F. Kostka, R. Schellenberg, F. Baitalow, T. Smolinka and F. Mertens, *Eur. J. Inorg. Chem.*, 2012, 49.

29 H. Erdogan, Ö. Metin and S. Özkar, *Phys. Chem. Chem. Phys.*, 2009, **11**, 10519.